AGU PUBLICATIONS

JGR

Journal of Geophysical Research: Biogeosciences

RESEARCH ARTICLE
10.1002/2015JG002983

Key Points:
- Organic layers on the ground surface protect underlying permafrost
- These layers need 500–700 years to recover after disturbance
- Topography and NDVI can be used to model soil surface organic layers in Alaska

Correspondence to:
C. A. Baughman,
cbaughman@usgs.gov

Citation:
Baughman, C. A., D. H. Mann, D. L. Verbyla, and M. L. Kunz (2015), Soil surface organic layers in Arctic Alaska: Spatial distribution, rates of formation, and microclimatic effects, *J. Geophys. Res. Biogeosci.*, *120*, 1150–1164, doi:10.1002/2015JG002983.

Received 4 MAR 2015
Accepted 6 MAY 2015
Accepted article online 14 MAY 2015
Published online 30 JUN 2015

Soil surface organic layers in Arctic Alaska: Spatial distribution, rates of formation, and microclimatic effects

Carson A. Baughman[1,2], Daniel H. Mann[3], David L. Verbyla[2], and Michael L. Kunz[2]

[1]Alaska Science Center, U.S. Geological Survey, Anchorage, Alaska, USA, [2]School of Natural Resources and Extension, University of Alaska Fairbanks, Fairbanks, Alaska, USA, [3]Department of Geosciences, University of Alaska Fairbanks, Fairbanks, Alaska, USA

Abstract Organic layers of living and dead vegetation cover the ground surface in many permafrost landscapes and play important roles in ecosystem processes. These soil surface organic layers (SSOLs) store large amounts of carbon and buffer the underlying permafrost and *its* contained carbon from changes in aboveground climate. Understanding the dynamics of SSOLs is a prerequisite for predicting how permafrost and carbon stocks will respond to warming climate. Here we ask three questions about SSOLs in a representative area of the Arctic Foothills region of northern Alaska: (1) What environmental factors control the thickness of SSOLs and the carbon they store? (2) How long do SSOLs take to develop on newly stabilized point bars? (3) How do SSOLs affect temperature in the underlying ground? Results show that SSOL thickness and distribution correlate with elevation, drainage area, vegetation productivity, and incoming solar radiation. A multiple regression model based on these correlations can simulate spatial distribution of SSOLs and estimate the organic carbon stored there. SSOLs develop within a few decades after a new, sandy, geomorphic surface stabilizes but require 500–700 years to reach steady state thickness. Mature SSOLs lower the growing season temperature and mean annual temperature of the underlying mineral soil by 8 and 3°C, respectively. We suggest that the proximate effects of warming climate on permafrost landscapes now covered by SSOLs will occur indirectly via climate's effects on the frequency, extent, and severity of disturbances like fires and landslides that disrupt the SSOLs and interfere with their protection of the underlying permafrost.

1. Introduction

Permafrost landscapes in the Arctic presently contain large amounts of organic carbon [*Tarnocai et al.*, 2009] and have acted as net sinks for atmospheric carbon through much of postglacial times [*McGuire et al.*, 2012]. Rapid warming of the Arctic could reverse this situation by triggering a permafrost-carbon feedback in which thawing allows the decomposition of organic matter that is now frozen, releasing more greenhouse gases to the atmosphere and further accelerating warming [*Schaeffer et al.*, 2011; *Hayes et al.*, 2014].

While it is unclear how quickly the permafrost-carbon feedback operates [*Schuur et al.*, 2015], we do know that the feedback is more complicated than warmer air temperatures simply causing more permafrost to thaw. Permafrost exists as an integral part of larger ecosystems whose various components mediate between aboveground and belowground climate [*Shur and Jorgenson*, 2007; *Schuur et al.*, 2008; *Johnson et al.*, 2013]. One of the most important of these mediating components is the mat of living plants and their decaying litter that covers the ground surface in many arctic regions [*Marchenko et al.*, 2008; *Treat et al.*, 2013]. In addition to comprising a substantial reservoir of stored carbon in their own right [*Tarnocai et al.*, 2009], the insulative effects of these soil surface organic layers (SSOLs) buffer the underlying permafrost and its contained carbon from changes in air temperature [*Jorgenson et al.*, 2010]. Such ecosystem-protected permafrost underlies large regions of North America and Eurasia [*Shur and Jorgenson*, 2007; *Johnson et al.*, 2013] and contains much of the permafrost carbon thought to be susceptible to the permafrost-carbon feedback [*Grosse et al.*, 2011]. A better understanding of arctic SSOLs is needed to predict how changing climate could affect the carbon stored in SSOLs, as well as the carbon stored in the permafrost they shield.

Soil surface organic layers are subject to several kinds of natural disturbances. These include centimeter-scale frost heaving [*Michaelson et al.*, 2008], decimeter-scale mass movements [*Jensen et al.*, 2014], and 100 km

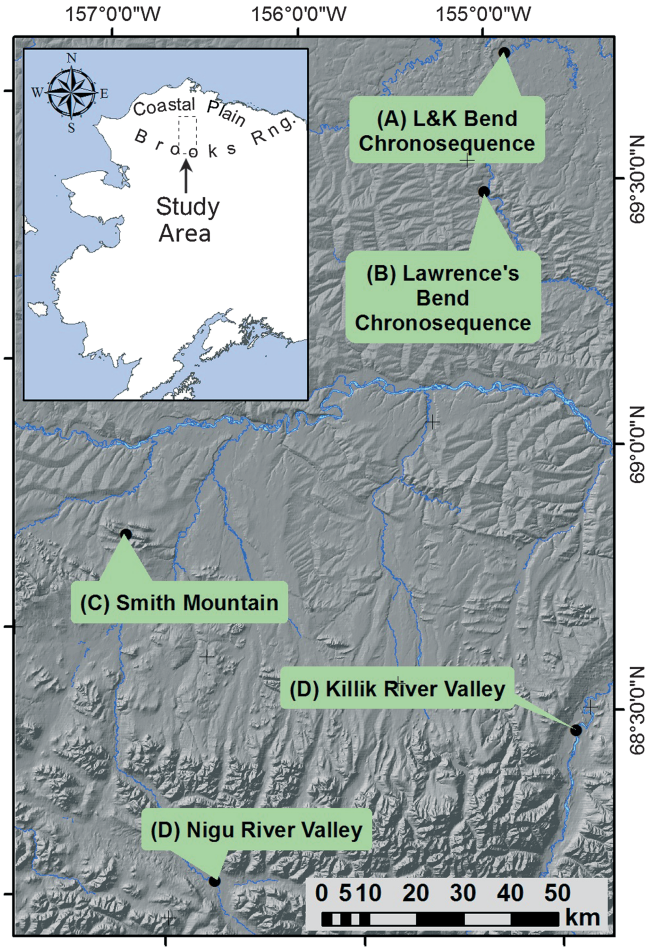

Figure 1. Map of study area. Inset depicts location of study area. (a) L&K Bend chronosequence along the Ikpikpuk River is the most northerly study site and lies on the northern edge of the Arctic Foothills province. (b) Lawrence's Bend chronosequence also located along the Ikpikpuk River. (c) Smith Mountain massif. See Figure 3 for additional details. (d) Nigu and Kilik River valleys are the location of multiple retrogressive thaw slumps.

scale fires [*Higuera et al.*, 2011; *Mack et al.*, 2011]. It takes time for SSOLs to recover after disturbances, and their thermal properties change over the course of recovery [*Jorgenson et al.*, 2010]. As a result, the SSOLs that cover permafrost landscapes are multiscale mosaics in which the mosaic pieces differ in how they were disturbed and in the time elapsed since last disturbance [*Walker et al.*, 2008; *Jones et al.*, 2013; *Raynolds et al.*, 2014].

To account for the inherent patchiness of arctic SSOLs when quantifying regional carbon stocks, computer models are needed that can incorporate the transient dynamics of SSOLs in a spatially explicit manner [*Mishra et al.*, 2013]. Computer models are also needed for predicting the responses of arctic carbon stocks to changing climate because of the large extent and complexity of soil geography in the Arctic [*Mishra and Riley*, 2012], the dynamic nature of organic carbon in near-surface layers of the ground there, and the scarcity of sampling [*Grosse et al.*, 2011; *Anthony et al.*, 2014]. With the ultimate goal of informing computer models of arctic carbon stocks, we ask three basic questions about soil surface organic layers in a representative area of the Arctic Foothills in northern Alaska, an ancient landscape underlain by continuous permafrost and possessing well-developed SSOLs distributed across complex topography. What environmental factors control its distribution? How long do SSOLs take to develop to equilibrium thicknesses on newly created geomorphic surfaces? What is the effect of SSOL cover on belowground temperatures?

2. Study Region

The Arctic Foothills lie between the Brooks Range and the Arctic Coastal Plain on Alaska's North Slope (Figure 1). Intense folding and erosion of sedimentary bedrock has produced steep, east-west trending ridges separated by rolling terrain now largely covered by low-, erect-shrub, and moist acidic tundra [*Walker*, 2000]. The foothills closest to the Brooks Range experienced four glacial advances over the last million years, the most recent ending ~14,000 years ago [*Briner and Kaufman*, 2008]. The foothills north of the Colville River were never glaciated and consist of rolling hills covered by shrub tundra and moist acidic tundra [*Walker et al.*, 1989; *Walker*, 2000]. Sedge- and shrub-dominated water tracks occur on many low-angle slopes, and willow shrubs form gallery thickets along streams. Soils in moist acidic tundra are Gelisols and include Typic, Rupic, and Histic Aquaturbels and Typic Mollihaplels, Typic Molliturbels, and Typic Histohaplels [*Bockheim et al.*, 1998]. Soils associated with moist nonacidic tundra include Typic Aquaturbels, Typic Histoturbels, and Typic Histohaplels [*Bockheim et al.*, 1998; *Ping et al.*, 1998]. While moist acidic tundra and moist nonacidic tundra are found within the Arctic Foothills region, our study sites are characterized by moist acidic tundra.

Climate in the Arctic Foothills is cold and relatively dry. Maximum summer temperatures reach 11–15°C and usually occur in July. Mean winter temperatures are between −29°C and −20°C. Mean annual precipitation is 14–19 cm, and total winter snow accumulation is 70–100 cm, with snowpack distribution being highly modified by wind [*Nowacki et al*., 2001]. The region is underlain by continuous permafrost, and the active layer (the upper layer of the ground that thaws and refreezes every year) is generally <1 m in thickness.

Our focus is on soil surface organic layers (SSOLs): mats of living and dead plant materials covering the ground surface. The term "peat" is reserved for SSOLs >30 cm thick [*Gorham*, 1991]. We use the term "SSOL" to distinguish it from other types of organic horizons commonly occurring in permafrost soils, including buried O horizons resulting from cryoturbation and mass movement [*Bockheim*, 2007].

We chose the Arctic Foothills as a place to study SSOLs because its complex topography affords a wide range of growing conditions with respect to available sunlight and moisture. In addition, meandering rivers in the Arctic Foothills have created soil chronosequences where vegetation, soil, and permafrost development can be observed over time in conjunction with SSOL development. Also, recently stabilized landslides provide sites where belowground temperature regimes can be monitored in SSOL-bare and SSOL-covered settings.

3. Study Sites

Smith Mountain is located 350 km south of Point Barrow in the Arctic Foothills and at latitude similar to Toolik Lake (Figure 1c). It consists of an unglaciated sandstone syncline of the Fortress Mountain Formation [*Molenaar et al*., 1988]. Kingak Mountain is the highest point on the massif at 905 m above sea level, while the lowest point is 364 m above sea level. Slope angles are gentle (0–5°) in the lowlands but reach 50° at higher elevations.

The Ikpikpuk River (Figures 1a and 1b) is a low gradient, meandering stream with a predominantly sand and gravel bed load. Its watershed covers 4400 km^2, and its mean annual discharge ranges between 11 and 29 $m^3 s^{-1}$. Peak flow usually occurs once per year as breakup floods in early June that promotes episodic cutbank erosion and meander scroll formation. Distant from the Brooks Range and lying north of the Colville River, the Ikpikpuk watershed has never been glaciated. Orderly sequences of meander scrolls of varying ages support successional seres extending from newly deposited sand and gravel to SSOL-covered tussock tundra and ice wedge polygons.

Geomorphic disturbances including retrogressive thaw slumps and sandy blowouts (Figure 2) are common in the valleys of the Nigu and Kilik Rivers, which flow northward from the Brooks Range (Figure 1d). The vegetation here consists of moist acidic tundra underlain by SSOLs 5–40 cm thick. Thaw slumps develop after some minor disturbance removes the overlying soil and exposes the underlying permafrost to the atmosphere [*French*, 2007]. Thaw then accelerates and exposes more permafrost. Slump activity is often episodic, with several years of quiescence followed by renewed activity. In steep terrain, thaw slumps can propagate upslope for decades [*Lantuit et al*., 2012]. The downslope, distal portions of these slides consist of barren mineral material (Figure 2) on which soil development begins quickly but proceeds slowly. The accumulation of plant litter can begin within 7 years following slumping, but chemical weathering requires 40+ years [*Burn and Friele*, 1989]. Permafrost either begins to aggrade as soon as the slump stabilizes or in some cases continues to degrade for several decades [*Niu et al*., 2012]. Thaw slumps provide the opportunity to compare soil temperature regimes under SSOL-free conditions with those under fully developed SSOLs developed in undisturbed vegetation nearby.

4. Methods

4.1. Environmental Factors Controlling SSOL Distribution and Related Carbon Stocks

We used multiple linear regression (MLR) to investigate the relationships between environmental parameters and SSOL thickness across the Smith Mountain massif [*Gessler et al*., 2000]. We chose topographic parameters for their potential influences on water availability and soil temperatures. Using a 5 m resolution, interferometric synthetic aperture radar-derived digital surface model [*Intermap*, 2010] and geospatial information software, we calculated parameter values for every 5 m × 5 m location within the study area. Parameters included slope (degrees), aspect (degrees), relative elevation (meters), upslope drainage area (25 m^2), profile curvature (curvature of slope parallel to the direction of the maximum slope—unit less),

Figure 2. Retrogressive thaw slump in the upper Nigu Valley. Data-logging station in foreground. Active thaw face in background with intact moist acidic tundra and soil surface organic layer (SSOL) beyond. Temperature logger and radiation shield is enclosed in a cage of hardware cloth to deter animal disturbance.

plan curvature (curvature of slope perpendicular to the direction of the maximum slope—unit less), curvature (combination of profile and plan curvature—unit less), accumulated direct solar radiation ($Wh\,m^{-2}$), accumulated diffuse solar radiation ($Wh\,m^{-2}$), relative duration of direct incoming solar radiation (hours), and a normalized difference vegetation index (NDVI—unitless). All radiation parameters are based on bihourly estimates of incoming solar radiation for 1 May to 31 September 2011. We employed a 2800 cell sky size, a 5 day interval, a 2 h interval, and a standard overcast sky setting for diffuse radiation. NDVI values were calculated from imagery acquired by the GeoEye-1 satellite (http://www.satimagingcorp.com/satellite-sensors/geoeye-1/) on 8 July 2010 at 21:59:03 UTC (image ID# 20100708215903OV05). This image offered the most cloud-free scene during peak growing season. The original 1.65 m resolution image was resampled to 5 m resolution and orthorectified to align with the digital terrain model of the Smith Mountain study area. NDVI was calculated using the near-infrared (NIR) wavelength (780–920 nm) and red (R) wavelength (655–690 nm) using the standard ratio, $(NIR - R)/(NIR + R)$.

We measured SSOL thicknesses in the field at 409 locations. Of these, 271 locations were dedicated to model calibration and were systematically located along 15 transects spanning the full range of each environmental parameter expressed within the study area (Figure 3). An additional 138 predetermined and randomly scattered locations, termed "test pits," were opportunistically sampled while traveling between model calibration locations (Figure 3). These 138 test pits were reserved for model testing. The global positioning system was used in the field to locate all sample locations with an accuracy of ±3 m. Soil pits approximately 0.1 m^2 in area were excavated using hand tools to the depth of mineral soil. We measured SSOL thickness as the distance between the bottom of living moss and the top of the uppermost mineral horizon.

Before inclusion in the MLR, parameters were tested for colinearity by calculating variance inflation factors [*Zuur et al*., 2010]. Parameters with the highest variance inflation factor (VIF) score were removed from the pool until all VIFs were < 3.0. The uncorrelated parameter data were combined with their associated SSOL thicknesses and included in the MLR. Forward selection was performed until all parameters were significant (p value < 0.05).

We used the resultant regression equation to calculate SSOL thickness for every 5 m × 5 m cell within the study area. We tested the model by comparing observed SSOL thickness with predicted SSOL thickness in the 138 test pits. We calculated root-mean-squared error (RMSE), coefficient of determination (R^2), and ratio of performance to deviation (RPD) to evaluate the overall performance of the SSOL model [*Gomez et al*., 2008].

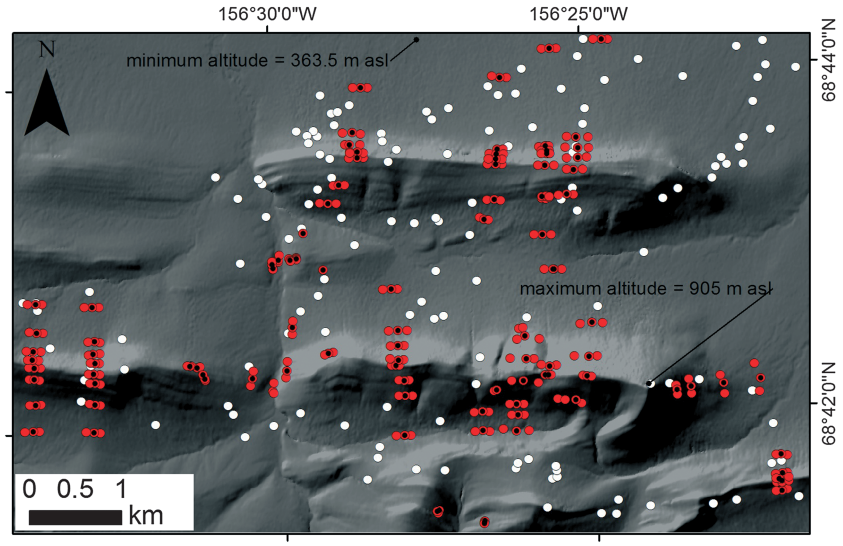

Figure 3. Sample design at Smith Mountain. Red dots indicate locations of model calibration pits ($n = 271$). Clusters of calibration pits are averaged together and represented by the central location (black points). These are termed model points ($n = 98$). White dots are the test pits ($n = 138$) used in testing the accuracy of model-estimated SSOL thickness.

4.2. Rates of SSOL Development

We identified two river bends along the Ikpikpuk River containing well-organized meander scroll sequences [*Nanson*, 1980] (Figure 4). We measured SSOL thicknesses along transects extending from the riverbank ($time = 0$) inland across progressively older meander scrolls to areas occupied by ice wedge polygons and moist acidic tundra. At the L&K site (Figure 4a), we dug soil pits in mid-July at every 5 m over the first 540 m and then at every 10 m over the next 380 m. At the Lawrence's Bend (LB) site (Figure 4b), we dug soil pits every 10 m in mid-July along a 350 m transect (Figure 4b). Additional soil pits were dug at the 628, 1117, and 1270 m marks. In each pit, we measured SSOL thickness to the nearest centimeter. Depth of thaw was measured to the nearest centimeter using three random probes with a tile probe within a 1 m radius of each soil pit. Shrub canopy height, canopy structure, understory species composition, and the relative dominance of different plant species were recorded at each sampling site. We dated the chronosequences using the radiocarbon (^{14}C) ages of the stems of in-growth position willow shrubs buried under point bar deposits and then reexposed in eroding cutbanks. Today, these buried stems can be found partially buried on active point bars and therefore are a good measure of when time equals zero.

Every meander scroll sequence develops through time along a different curvilinear trajectory (Figure 4). This means that the straight line distance from the currently active point bar is not a useful indicator of relative age. A more meaningful metric is the relative position of each sampling site with respect to the accretion axis of the scroll sequence [*Hicken*, 1974]. The primary accretion axis reflects the long-term growth pattern of the point bar, and it is defined as the point on each meander scroll where the orthogonals to the scroll crests can be divided approximately bilaterally [*Hicken*, 1974]. Once the accretion axis was defined, we projected all sample data onto that axis. To assign ages to specific points along this axis, we traced the scroll ridges and swales under which the ^{14}C-dated willows originated laterally to where they intercepted the primary accretion axis. The same was done for a number of reference points along the sampling transect. CLAM version 2.1 software and the smooth spline model [*Blaauw*, 2010] was used to infer ages for successive positions along the accretion axis, while a simple linear interpolation equation was used to convert all the remaining distances along the transection to distances on the accretion axis.

4.3. Effects of SSOLs on Belowground Temperature

To investigate how the presence of a SSOL affects belowground temperature regimes, we measured air and mineral soil temperature over the course of a year at sites that were SSOL free, SSOL developing, or SSOL covered. The eight ($n = 8$) SSOL-free sites consisted of five retrogressive thaw slumps in the Nigu River valley, one blowout in tundra-covered sand dunes along the Kilik River, and two vegetation-free point bars

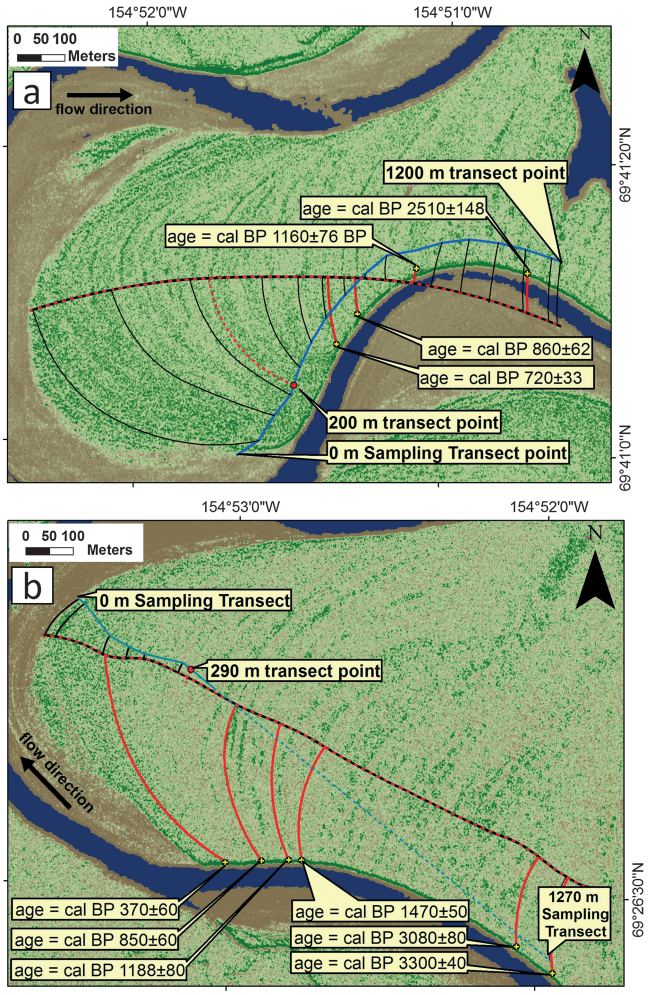

Figure 4. (a) The L&K chronosequence. Brown areas are the actively depositing portions of point bars. Soil sampling points lie along the blue transect lines. Yellow dots show locations of ^{14}C samples collected along cutbanks. Location of soil samples and ^{14}C sample sites are projected onto the primary accretion axis (dashed line) based on meander scroll patterns. (b) The Lawrence's Bend chronosequence. Brown areas are the actively depositing portions of point bars. Soil sampling points lie along the blue transect lines. Yellow dots show locations of ^{14}C samples collected along cutbanks. Location of soil samples and ^{14}C sample sites are projected onto the primary accretion axis (dashed line) based on meander scroll patterns.

along the LB chronosequence on the Ikpikpuk River. The 15 ($n = 15$) SSOL-covered sites consisted of five locations of undisturbed, moist acidic tundra vegetation adjacent to each of the five thaw slump sites in the Nigu Valley, one herbaceous tundra location adjacent to the sand blowout in the Kilik Valley, five locations along the vegetated scrollbar surfaces of the LB chronosequence, and four locations located on low-angle, moist acidic tundra on each cardinal flank of Smith Mountain.

Each monitoring site was instrumented with two temperature loggers (onset HOBO model UA-001-08, Pocasset, MA, USA) that recorded air and soil temperature bihourly. These loggers have a reported accuracy of ±0.53°C from 0 to 50°C and a recommended operating range of −20 to 70°C. Temperatures at the thaw slumps, the sand blowout, and along the LB chronosequence were recorded for 1 year (June 2011 to August 2012), while temperatures at the Smith Mountain sites were recorded during June–August 2012. At SSOL-covered sites, air temperature was recorded 8–10 cm above the surface of the moss layer within a radiation shield. Belowground temperature was measured at the organic/mineral interface. At SSOL-free locations, air temperature was measured 8–10 cm above the exposed mineral soil surface, and soil temperature was measured 2–4 cm below the exposed mineral soil surface. Along the LB chronosequence, data loggers were located at 0, 40, 100, 150, 190, 270, and 1200 m inland along the sampling transect. At all sites in all study areas, two sets of temperature loggers were used for replicate measurements and were placed 10–20 m apart.

5. Results

5.1. Modeling Distribution of SSOLs on Smith Mountain

We found the mean SSOL thickness at all sample locations to be fairly uniform: 8.0 ± 5.6 cm (±1 standard deviation (SD)). Minimum and maximum observed SSOL thicknesses were 0 and 26 cm, with SSOL-free areas occurring on steep slopes (>40°), ridge tops, scree fields, and in areas disturbed by animal digging.

For MLR construction, all parameters were found to be approximately normally distributed except upslope area, which was transformed using a log transformation ($\log_{10}(x)$). Topographic parameters that we found to be sufficiently uncorrelated with one another included duration of direct radiation, accumulated direct

Table 1a. Multiple Linear Regression Output[a]

Parameters	Estimate	Standard Error	*t* Value	PR(> *t*)
(Intercept)	−1.105	6.004	−0.184	0.854
Relative elevation	−0.026	0.005	−5.052	21e−6
Upslope area	1.694	0.775	2.187	0.031
NDVI	20.45	8.493	2.408	0.018
Direct radiation	−0.000008	0.000004	−1.682	0.0959

[a]Output depicts correlative relationship between environmental parameters and SSOL thickness (cm).

radiation, profile curvature, plan curvature, upslope drainage area, relative elevation, aspect, and NDVI. To dampen the small-scale noise in SSOL thicknesses that is common in organic-rich landscapes [*Parry et al.*, 2012], we resorted to averaging neighboring sample locations together to produce 98 "model points." This yielded the following best fitting regression equation (equation (1)):

$$Y = -0.003(e) + 1.694(a) + 20.45(N) - 0.000008(d) - 1 \quad (1)$$

Y SSOL thickness, cm;
e relative elevation, m;
a upslope drainage area, 25 m^2;
N NDVI, unitless;
d direct radiation received between May and September 2011, Wh m^{-2}.

Using these parameters yielded an overall, adjusted R^2 of 0.52 and an overall p value of 3.2×10^{-15} (Tables 1a and 1b). Based on p values, relative elevation was the variable most significantly correlated with variation in SSOL thickness. NDVI is the next most significant parameter, followed by upslope-drainage-area and direct radiation, respectively. An increase in direct solar radiation or relative elevation accompanies thinner SSOLs, while an increase in NDVI and upslope-drainage-area is associated with an increase in SSOL thickness.

The regression equation (equation (1)) was then used to estimate SSOL thickness for every 5 m × 5 m cell within the study area. We found that we could use NDVI values *d* to mask areas that were vegetation free. Any cells with an NDVI value less than 0.63 were automatically assigned a 0 cm SSOL thickness. All remaining SSOL estimate values were rounded to the nearest centimeter.

Model testing found minimal agreement between observed and predicted SSOL thicknesses in the 138 test pits. The mean error of the estimate for all 138 test pits was 1.01 cm of SSOL; however, the RMSE was 70.02 cm. The coefficient of determination (R^2) equaled 0.20. The calculated RPD was 0.04, which suggests the model has little to no predictive abilities at the scale of 5 m [*Chang and Laird*, 2002].

Our model performs adequately at larger spatial scales but poorly at smaller ones (Figure 5). Specifically, the model correctly highlights areas of thin or absent SSOLs through the use of the NDVI threshold thereby accurately modeling the SSOL-free nature of ridgelines, scree fields, and high-elevation areas. Water tracks (linear, downslope-oriented swales with perennially saturated soils and substantial organic layers) stand out as locations with thicker SSOLs. The model also yields a realistic estimate of total SSOL thickness. The observed average SSOL thickness for the test pits is similar to modeled average SSOL thickness, 11.3 ± 6.7 cm versus 10.3 ± 3.0 cm, respectively (±1 SD).

Table 1b. Multiple Linear Regression Output[a]

		Values
Residuals		−9.8
	1Q	−2.2
	Median	−0.3
	3Q	2.2
	Max	9.1
Multiple R^2		0.5414
Adjusted R^2		0.5219
F statistic		27.74 on 3 and 94 DF
p value		3.232e−15

[a]Output reports measure of goodness of fit.

5.2. Carbon Stocks Inferred From Modeled SSOL Thickness

The SSOL thickness model, while weak, can be used to estimate the amount of organic carbon stored at the soil surface on a regional basis and demonstrates one future application

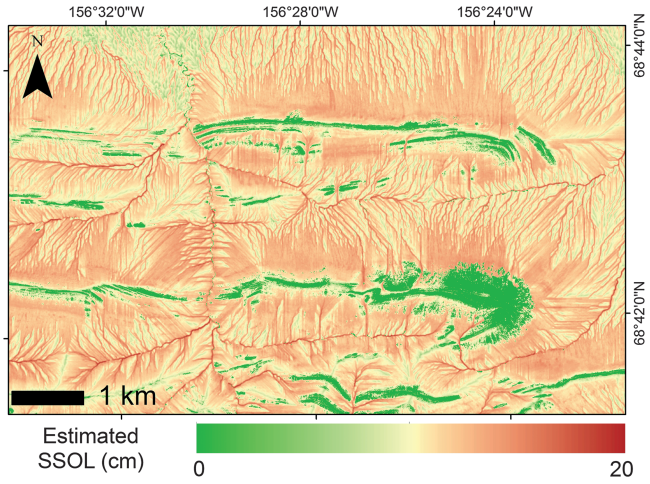

Figure 5. At large spatial scales, the model successfully simulates the natural patterns SSOLs on Smith Mountain. Specifically, SSOLs are absent or thin on ridge tops, steep slopes, and at high elevations. SSOLs >17–18 cm are restricted to water tracks and the thickest SSOLs occur where water tracks converge to form first-order drainages.

of similar models. A close relationship exists between SSOL thickness and SSOL-based soil organic carbon density in the Arctic Foothills (Figure 6, equation (2)) due to the regional uniformity of bulk density within surficial organic layers [*Michaelson et al*., 2013].

$$\text{SSOL kg C m}^{-2} = 0.68(Y) r^2 = 0.80, \quad p \text{ value} = << 0.01, \; n{=}35 \qquad (2)$$

These relationships are based on the Arctic Foothills samples ($n = 35$) from the most recently cataloged University of Alaska and U.S. Department of Agriculture-Natural Resources Conservation Service soil profiles [*Michaelson et al*., 2013]. Applying equation (2) to the SSOL thickness model output results in an overall estimate of 0.45 ± 0.06 Tg of C occurring within SSOLs in the entire Smith Mountain study area. Estimated SSOL-based carbon stocks ranged from 0 to 15 kg C m^{-2} with a weighted average of 9.55 kg C m^{-2} and a standard deviation of 2.46 kg C m^{-2}.

5.3. Chronology of SSOL Development

The point bar chronosequences (Figure 4) are useful for estimating how long SSOLs take to develop and reach steady states. The oldest parts of the LB and L&K transects date to 3300 ± 40 cal years B.P. and 2510 ± 130 cal years B.P., respectively (Table 2). Vegetation succession is similar along both chronosequences. Immediately adjacent to the sandy point bar, vegetation is sparse and sand and/or gravel is widely exposed. The plants growing here include grasses, forbs, and scattered willow shrubs. Within the first 100 m inland from the shoreline, willow shrubs form a thicket up to 3 m high. Ground layer vegetation is still patchy and consists of mosses, *Equisetum*, and forbs. Moving inland, the ridge and swale topography of the meander scrolls produces small-scale variations in plant communities. On the meander scroll ridges, dense stands of low willow and ericaceous shrubs occur. Sedges dominate in the swales. Further inland, 150 to 170 m from the active part of the point bar, dwarf shrub tundra becomes widespread. This vegetation persists until ice wedge polygons develop under moist acidic tundra vegetation near the end of each transect.

In addition to the changes in vegetation just described, marked changes in soil development, SSOL thickness, and depth of thaw occur along both chronosequences. At the L&K site, organic layer accumulation begins in isolated patches around 45 m inland at a point with an estimated age of <10 years (calibrated years before 2010 Common Era (C.E.)). These scattered patches of SSOL consist of mosses, herbs, grasses, and/or willow leaves. A thin SSOL develops in swales around 85 m inland and consists of thin, alternating bands of buried litter and silt deposited during occasional floods. This location is estimated to be 110 ± 10 years (±1 SD). A continuous organic soil horizon first appears around 100 m inland, which has an estimated age of 170 ± 10 years. Depth of thaw decreases simultaneously in an erratic fashion (Figure 7). The trend of thickening organics and thinning depth of thaw continues until approximately 200 m from the active point bar, where

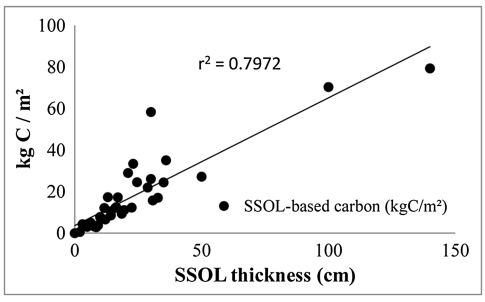

Figure 6. Relationship between SSOL thickness and SSOL carbon stocks. Shown here are results from 35 soil pits within the Arctic Foothills (redrawn using data of *Michaelson et al*. [2013]).

Table 2. Radiocarbon (^{14}C) Dates From the Ikpikpuk River Valley

Field Number	Lab Number Beta-######	Location Latitude (°N), Longitude (°W)	Dated Material	$\delta^{13}C$ (‰)	^{13}C-Normalized Age (Years Before 1950 C.E.)	1 Standard Deviation	2 s Calibrated Age Range (cal years B.P.)	Mean Probable Calibrated Age (cal years B.P.)
			Lawrence's Bend					
LBEND14	311696	69°26.5′, 154°53.0′	Willow in-growth position (WGP)	−29.0	310	30	301:463	380
LBEND13	315152	69°26.5′, 154°52.9′	WGP	−27.0	920	30	766:922	840
LBEND12	315151	69°26.5′, 154°52.8′	WGP	−26.4	1240	30	1077:1264	1170
LBEND11	311695	69°26.5′, 154°52.8′	WGP	−27.5	1580	30	1403:1535	1470
LBEND03	311694	69°26.4′, 154°52.0′	WGP	−29.1	2930	30	2973:3208	3090
LBEND01	311693	69°26.4′, 154°51.9′	WGP	−27.4	3070	30	3215:3362	3290
			L&K Bend					
LK17	331699	69°41.1′, 154°51.3′	WGP	−29.8	900	30	739:910	820
LK16	331696	69°41.1′, 154°51.3′	WGP	−27.8	1000	30	798:967	1070
LK15a	331698	69°41.2′, 154°51.1′	WGP.	−27.1	1260	30	1088:1281	1180
LK7a	331697	69°41.2′, 154°50.7′	WGP	−28.9	2490	30	2368:2725	2550
LK7b	331694	69°41.2′, 154°50.7′	Basal 2 cm of 20 cm thick peat layer covering LK7a	−28.7	990	30	797:961	880

they both reach steady states. At this point, where surface age is 550 ± 50 years, we consider the SSOL to have reached a steady state. Beyond this point along the L&K chronosequence, both SSOL thickness and depth of thaw remain relatively constant (Figure 7).

At the LB site, soil organic accumulation follows a similar pattern as at L&K. Surface organics begin to accumulate 20 m inland of the barren surface of the active point bar. The 20 m mark is estimated to be 20 ± 4 years old. A pronounced surface organic horizon has developed around 70 m inland at a position estimated to be 260 ± 50 years old. The depth of thaw thins erratically until approximately the 290 m point where it begins to stabilize. This location is estimated to be 720 ± 60 years old and represents the point where SSOL reaches a steady state (Figure 7).

5.4. Effects of SSOLs on Ground Temperatures

The six SSOL-covered sites in the Nigu and Kilik Valleys had a mean SSOL thickness of 13 ± 2 cm (±1 SD). At the temperature monitoring sites on Smith Mountain, the mean SSOL thickness was 17.4 ± 1.7 cm. A *z* test

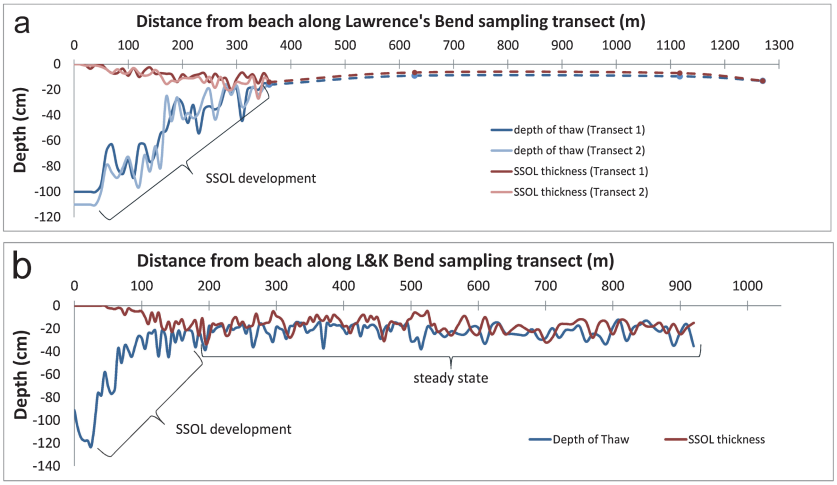

Figure 7. (a) Relationship between SSOL thickness and distance from active point bar in the Ikpikpuk Valley. SSOL formation initiates quickly, stabilizes around 300 m, and then maintains a steady state. Arrows represent radio carbon dates. (left to right) 20 ± 4 years B.P., 260 ± 50 years B.P., 720 ± 60 years B.P., and 3300 ± 40 years B.P. (b) Relationship between SSOL thickness and distance from active point bar in the Ikpikpuk Valley. SSOL formation initiates quickly, stabilizes after 200 m, and then maintains a steady state. Arrows represent radio carbon dates. (left to right) <10 years B.P., 110 ± 10 years B.P., 170 ± 10 years B.P., 550 ± 50 years B. P., 2510 ± 130 years B.P.

Table 3. Summary of Bihourly 2011–2012 Temperature Data[a]

	Max Growing Season		Peak Growing Season	
	Bare	Tundra	Bare	Tundra
Mean air temperature	4.9 ± 0.6	4.7 ± 0.1	10.9 ± 0.7	11.0 ± 0.3
# of days air temperature >0°C	126 ± 10	127 ± 17	92 ± 0	92 ± 0
Air growing degree days > 0°C	1154 ± 111	1225 ± 66	1000 ± 62	1013 ± 28
Mean ground temperature °C	5.4 ± 1.3	0.8 ± 0.5	10.9 ± 1.2	2.5 ± 0.9
# of days ground temperature >0°C	131 ± 4	131 ± 4	92 ± 0	84 ± 5
Ground growing degree days > 0C	1168 ± 169	263 ± 85	1005 ± 107	230 ± 80
Mean thermal advantage (degree days)	−31 ± 202	962 ± 107	−13 ± 124	783 ± 85

[a]Bare: location of exposed mineral soil within retrogressive thaw slumps ($n = 5$). Tundra: location covered in 13 ± 1 cm of SSOL adjacent to thaw slumps ($n = 6$). Max growing season = May, June, July, August, September, and October. Peak growing season = June, July, and August. Growing degree day: (air or ground degree days >0°C). Thermal advantage: average difference between air and ground growing degree days.

comparing mean air temperatures inside and outside of the five retrogressive thaw slump sites in the Nigu Valley from June through August found no significant difference ($\alpha = 0.01$, p value = 0.32). Hence, we assume that differences seen in mineral soil temperatures inside and outside retrogressive thaw slumps were caused by the presence of SSOLs.

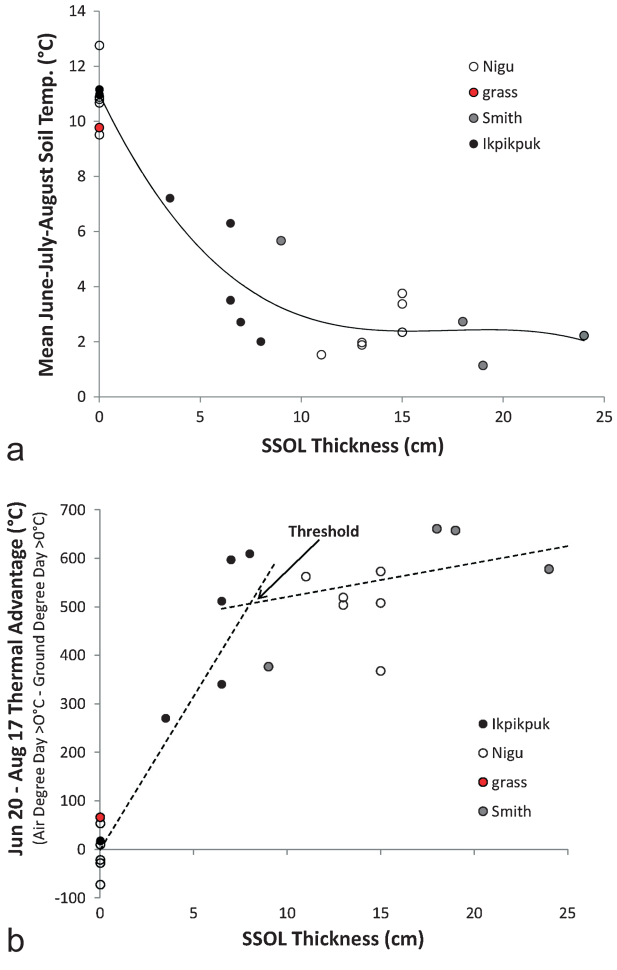

Figure 8. (a) Influence of SSOL thickness on mean June-July-August mineral soil temperature. A threshold exists in the relationship between SSOL thickness and the temperature of the underlying mineral soil when SSOLs reach about 7 cm in thickness. (b) SSOL thickness and the thermal advantage. Thermal advantage is the difference in accumulated growing degree days between the air and soil environment.

The presence of SSOLs was associated with lower monthly mean soil temperature at the organic/mineral interface (Table 3). June, July, and August mean soil temperatures (MSTs) were reduced by 10.3 ± 1.1°C, 9.1 ± 0.8°C, and 5.7 ± 0.6°C, respectively (± = standard error of mean). This resulted in under SSOL MSTs for June, July, and August of 1.2 ± 0.5°C, 3.3 ± 0.4°C, and 2.9 ± 0.2°C, respectively. The presence of SSOLs lowered mean soil temperature for June, July, and August by 8.3 ± 0.7°C and resulted in a mean, growing season temperature (May–October) that was 4.4 ± 0.6°C lower. Temperature measurements from all study sites show that an increase in SSOL thickness strongly correlates with a decline in growing season soil temperature (Table 3).

The presence of a SSOL also strongly affected growing degree days (GDDs) at the mineral soil surface. Under climax-state SSOLs (i.e., intact, mature tundra vegetation), total summer growing season GDDs (accumulated daily mean temperature > 0°C) at the organic/mineral soil interface totaled 263 ± 85°C compared to 1168 ± 169°C at a 2 cm depth in bare mineral soil (Table 3). This equates to a reduction of available heat energy by 77%.

The effect of an SSOL cover on belowground growing conditions is a nonlinear function of SSOL thickness. The difference in GDDs above and belowground increases as SSOLs accumulate, up to a thickness of about

7 cm. After 7 cm is reached, the rate of change in the difference declines (Figure 8). This implies that 7 cm of SSOL has nearly the same biologically relevant cooling effect as 15 or 30 cm of SSOL.

6. Discussion

6.1. Predicting SSOL Distribution and Thickness

The middling correlation between SSOL formation and topographic parameters ($R^2 = 0.52$) is comparable to the results of other models that predict soil characteristics based on terrain parameters. For example, *Gessler et al*. [1995] predicted solum and A horizon depths in Australia using a regression model with R^2 values between 0.63 and 0.68. In Taiwan, *Tsai et al*. [2001] predicted B horizon thicknesses based on slope angle in a model with R^2 values as low as 0.05. In Labrador, *Graniero and Price* [1999] predicted vegetation distribution in a bog using a regression model with an R^2 of 0.22. *Parry et al*. [2012] predicted peat volume and carbon stores on the Dartmoor using R^2 values ranging from 0.27 to 0.54. Despite these moderate to low R^2 values, each of these authors found their model capable of practical application. R^2 values alone are not a sole indicator of a predictive model's accuracy [*Zuur et al*., 2010], and the direct comparison of model predictions with reserved sets of validation data offers an alternative assessment of model capability.

In this case, comparison of the predicted and validation data sets indicates poor predictive capabilities at small spatial scales within the study area (coefficient of determination (R^2) = 0.2; ratio of performance to deviation (RPD) = 0.04). In contrast, our model is more successful at predicting SSOL thicknesses at larger spatial scales and can usefully depict the distribution of SSOL thickness in relation to topography and elevation on real landscapes. Specifically, the model finds that sites on Smith Mountain that are free of vegetation lack SSOLs and that water tracks possess the thickest SSOLs (Figure 5). It also yielded a realistic estimate of total SSOL thicknesses in the Smith Mountain study area. Additional sampling efforts would be required to validate model accuracy at the larger scale and an approach similar to *Pastick et al*. [2014] would be required for the assessment of the entire Arctic Foothills region.

What causes our model's inaccuracy at small spatial scales? The underlying reason probably relates to the geomorphic stochasticity inherent to many periglacial landscapes. The slopes of Smith Mountain are a mosaic of small-scale disturbances including solifluction lobes, mud boils, and ice wedge polygons. Together these disturbances have created a microtopographic mosaic whose pieces vary in time since last disturbance. This in turn creates a mosaic of plant communities under which SSOLs accumulate at varying rates. Because there is only a limited range in SSOL thicknesses in the Smith Mountain study area and because these SSOL thicknesses are relatively noisy, the resultant model fails at small spatial scales even while it succeeds at larger ones. In hindsight, a more extensive survey that included more sites supporting thicker SSOLs may have improved the signal-to-noise ratio and allowed better model building. At present, small-scale heterogeneity caused by the spatial mosaic of periglacial disturbances probably dooms any attempts to model SSOL thicknesses as a continuous variable at spatial scales < 50 m. *Pastick et al*. [2014] successfully estimates binary organic layer thickness at the 30 m scale using an exceptionally large number of observations within the Yukon River Bain. *Mishra and Riley* [2012] also successfully model categorical soil carbon stocks at the 60 m scale. In time, it is likely that high-resolution data sets concerning soil-forming factors will be paired with the ever-growing database of soil observation making accurate high-resolution ($<$50 m) predictive models possible.

6.2. How Realistic Are These Soil Carbon Estimates?

Direct comparisons with previous estimates of soil carbon stocks in other permafrost areas are difficult because our focus here is on SSOL carbon within a single landscape. Previous work has often partitioned the soil carbon pool into generalized layers (e.g., active layer versus permafrost) and stratified the entire Arctic into generalized landscape units (e.g., uplands, mires, and tundra). Our topographic- and NDVI-based model estimates that 0.45 ± 0.06 teragrams (Tg) of carbon exists in SSOLs within the 47 km^2 Smith Mountain study area ($\pm$ = 95% confidence interval (CI)). This equates to 9.49 ± 1.18 kg C m^{-2}, which is in the range of previous estimates for similar arctic regions (Table 4).

6.3. Development of Steady State SSOLs

On floodplains in the Arctic Foothills, organic matter begins to accumulate on the ground surface within several decades following point bar stabilization, the point when the point bar becomes largely isolated

Table 4. Previous Carbon Stock Estimates for Similar High-Latitude Regions

Author	Landscape/Region	kg C/m^2
Kurz et al. [1992]	Arctic soils	17.1
Kurz et al. [1992]	Subarctic soils	33.8
Shaver et al. [1992]	North America tundra	22
Gilmanov and Oechel [1995]	North American tundra uplands	20.95
Tarnocai [1998]	Average North American Arctic, mineral soil	12
Tarnocai [1998]	Average North American Arctic, organic soil	43
Ping et al. [2008]	Upland O-enriched surface horizons	7.5 ± 11.6
Tarnocai et al. [2009]	Circum-Arctic Gelisols to 1 m depth	22.6–66.6
Johnson et al. [2011]	Arctic Alaska upland tundra, surficial organic layers	5.9–8.8
Johnson et al. [2011]	Arctic Alaska lowland tundra, surficial organic layers	3.7–4.0
Johnson et al. [2011]	Arctic Alaska upland tundra to 1 m depth	42.4–72.9
Johnson et al. [2011]	Arctic Alaska lowland tundra to 1 m depth	34.3–35.3
Michaelson et al. [2013]	Arctic Alaska entisols	1.31[a]
Michaelson et al. [2013]	Arctic Alaska gelisols	1.01[a]
This study	Smith Mountain, Arctic Foothills	9.49 ± 1.18

[a]Average density per centimeter SSOL thickness.

from annual floodings. The developing SSOLs eventually reach a steady state thickness after 500–700 years. Organic accumulation occurs rapidly at first and then slows. Microtopography created by the underlying meander scroll topography and by ice wedge polygons affects SSOL development. Namely, SSOLs develop soonest and thicken fastest in the swales, while on scroll crests SSOLs are slower to form and remain relatively thin. Microtopography is an important factor in controlling SSOL development on the floodplain just as it is on the slopes of Smith Mountain.

A steady state in SSOL thickness is reached when the addition of new plant litter is matched by the combined actions of decomposition, cryoturbation, and lateral transfer by wind or burning. As a result, a SSOL's basal ^{14}C age can be significantly younger than the age of the underlying geomorphic surface. At one location along the L&K chronosequence, a willow buried in river sand beneath the SSOL dated to 2550 years, while the basal age of the 20 cm thick SSOL on the ground surface above it dated to only 880 years (Table 2), suggesting that the first 1700 years of accumulated C was lost to decomposition, cryoturbation, or lateral transfer. The maintenance of a mass balance between gains and losses of organic matter is consistent with the fluctuating, steady state in SSOL thicknesses observed along the two floodplain chronosequences (Figure 7). Our chronosequence study sites are typical of the immediate region, but additional replicate studies from adjacent river systems would be valuable for substantiating and improving our estimates.

6.4. Soil Surface Organic Layers and Ecosystem-Protected Permafrost

Soil surface organic layers play several important ecological and geomorphic roles in the Arctic Foothills. First, they store a large amount of carbon (1.0–1.7 kg C m^{-2} cm^{-1} (Table 4)), which accounts for 35 ± 21% of the total carbon contained in the top meter of soil profiles in the Arctic Foothills [*Michaelson et al.*, 2013]. Second and perhaps more importantly, SSOLs help maintain ecosystem-protected permafrost in the ground below [*Shur and Jorgenson*, 2007]. At our study sites, the presence of a SSOL >7 cm thick reduced mean June-July-August soil temperatures at the top of the mineral soil by 8°C (Figure 8). This cooling maintains thinner active layers and colder permafrost.

The presence of a SSOL relies on the existence of a "thermal advantage" between the ground surface where plants are fixing carbon and below the surface where these carbon compounds are being decomposed [*Swanson et al.*, 2000]. Soil temperatures below 0°C retard belowground decomposition, and cooling below −6°C reduces it to very low rates [*Price and Sowers*, 2004; *Panikov et al.*, 2006]. Following the stabilization of new geomorphic surfaces after a disturbance like a fire or a landslide that restarts primary succession, the ground surface can either possess a slight thermal advantage (it is warmer) or a slight disadvantage (it is colder) than the underlying mineral soil. Our results show that within our study area and under the present climate of the Arctic Foothills, the accumulation of even a thin layer of plant litter endows the ground surface with a thermal advantage over the mineral soil, which then triggers a positive feedback encouraging the accumulation of more organic material. This process accounts for the ubiquitous nature of SSOLs within our study area.

Our measurements show that within our study sites, the thermal advantage of the ground surface increases steadily as SSOLs accumulate up to a thickness of about 7 cm (Figure 8). After this thickness is reached, the rate of increase in thermal advantage per increase in SSOL thickness declines. This suggests that the accumulation of SSOL in excess of 7 cm may be largely irrelevant to biological activity in the underlying mineral soil.

6.5. SSOLs and Warming Climate

SSOLs in the Arctic Foothills exist at the front line of climate change for several reasons. Small shifts in aboveground climate can alter the balance between plant productivity and microbial decomposition that determines the mass balance of organic carbon in SSOLs. Furthermore, because SSOLs are at the ground surface, they are vulnerable to ecological disturbances like wildfires [*Mack et al*., 2011; *Higuera et al*., 2011; *Jones et al*., 2013], which in turn are strongly influenced by summer climate [*Hu et al*., 2010]. There are indications that tundra fires are becoming more frequent in the Arctic Foothills [*Hu et al*., 2010; *Chipman et al*., 2015]. Although the frequencies of tundra fires are still poorly resolved in Arctic Alaska, they appear to range between several decades to >500 years depending on topography and vegetation type [*Higuera et al*., 2011; *Jones et al*., 2013; *Chipman et al*., 2015].

The dynamics of SSOLs could prove crucial to permafrost stability and carbon storage if fires become more frequent. This follows from the observations along the Ikpikpuk chronosequences that 250–300 years are required for SSOLs to reach the critical 7 cm thickness and 500–700 years to reach steady states. If fire return intervals shorten to 200–300 years, SSOLs will have difficulty accumulating, and widespread thermokarsting and release of permafrost carbon could result.

7. Conclusions

1. *Spatial variation in thickness of soil surface organic layers* (*SSOLs*). Topography and vegetation productivity can be used to predict SSOL thickness and distribution in Arctic Alaska at spatial scales greater than ~1 km. The most important topography-related factors are relative elevation, upslope drainage area, and direct radiation. Together with NDVI, these factors explain 52% of the variation in SSOL thickness and provide a way to remotely model SSOL-carbon distribution in regions of complex topography with climates similar to the Arctic Foothills.
2. *Belowground Carbon Stocks*. Our model estimates that the 47 km^2 Smith Mountain study area contains approximately 0.45 ± 0.06 Tg or 9.49 ± 1.18 kg C m^{-2} in its SSOLs ($\pm$ = 95% CI).
3. *Rates of SSOL Formation*. On river floodplains in the Arctic Foothills, SSOLs begin to accumulate 5–20 years after a new geomorphic surface stabilizes and require 500–700 years to reach steady state thicknesses. These rates are for SSOL formation on sandy, low-angle, lowland surfaces. Rates of SSOL development are probably slower on steep slopes underlain by coarser parent material and faster on silty, moist substrates.
4. *SSOL Feedbacks on Soil Temperature*. The presence of a SSOL significantly cools the underlying mineral soil and, by doing so, buffers the underlying permafrost from warming air temperatures. The presence of a mature SSOL reduces mean annual soil temperature at the SSOL/mineral interface by 3°C. Its presence also reduces growing degree days (degree days > 0°C) within the mineral soil by nearly 80%. In the Arctic Foothills today, SSOL formation is primed to begin as soon as the ground surface stabilizes after a disturbance like a deeply burning fire or a landslide. The accumulation of any insulating, organic material on the ground surface quickly shifts the thermal advantage to aboveground productivity and triggers a positive feedback loop favoring SSOL accumulation.
5. *Vulnerability of SSOLs to changing climate*. Because they protect permafrost from warm air temperatures, disruption of SSOLs may be the proximate link between warming climate and widespread permafrost thaw in the Arctic Foothills. The permafrost-buffering effects of SSOLs in the Arctic Foothills are probably particularly sensitive to fires, whose frequency is predicted to increase as summer climate warms. Fire return intervals less than 200–300 years may represent a crucial threshold leading to significant increases in the release of carbon now stored in permafrost.

Acknowledgments
This research was supported by the Alaska Climate Science Center, through Cooperative Agreement G10AC00588 from the United States Geological Survey, National Science Foundation grant ARC-0902169, and by the University of Alaska, Fairbanks Scenarios Network for Alaska and Arctic Planning (SNAP; www.snap.alaska.edu). Logistical support in the field came from the Bureau of Land Management's Arctic Field Office. We thank Connie Adkins, Pamela Groves, Curt Baughman, Amy Breen, and Nickoli Kalman for their assistance in the field. We thank Ben Jones, Miriam Jones, Stephen Tooth, Gary Michaelson, Dave Valentine, and Chen Liu Ping for technical support and stimulating discussions. All data are available upon request. The views and conclusions contained in this document are those of the authors and should not be interpreted as representing the opinions or policies of the USGS or the U.S. Government. Use of trade, product, or firm names is for descriptive purposes only and does not imply endorsement by the U.S. Government.

References

Anthony, K. M. W., et al. (2014), A shift of thermokarst lakes from carbon sources to sinks during the Holocene epoch, *Nature*, *511*, 452–456.
Blaauw, M. (2010), Methods and code for "classical" age-modeling of radiocarbon sequences, *Quat. Geochronol.*, *5*, 512–518.
Bockheim, J. G. (2007), Importance of cryoturbation in redistributing organic carbon in permafrost-affected soils, *Soil Sci. Soc. Am. J.*, *71*, 1335–1342.

Bockheim, J. G., D. A. Walker, K. R. Everett, E. E. Nelson, and N. I. Shiklomanov (1998), Soils and cryoturbation in moist nonacidic and acidic tundra in the Kuparuk River Basin, Arctic Alaska, U.S.A, *Arct. Alp. Res.*, *30*, 166–174.
Briner, J. P., and D. S. Kaufman (2008), Late Pleistocene mountain glaciation in Alaska: Key chronologies, *J. Quat. Sci.*, *23*, 659–670.
Burn, C. R., and P. A. Friele (1989), Geomorphology, vegetation succession, soil characteristics and permafrost in retrogressive thaw slumps near Mayo, Yukon Territory, *Arctic*, *42*, 31–40.
Chang, C. W., and D. A. Laird (2002), Near-infrared reflectance spectroscopic analysis of C and N, *Soil Sci.*, *167*, 110–116.
Chipman, M. L., V. Hudspith, P. E. Higuera, P. A. Duffy, R. Kelly, W. W. Oswald, and F. S. Hu (2015), Spatiotemporal patterns in tundra fires: Late-Quaternary charcoal records from Alaska, *Biogeosci. Discuss.*, *12*, 3177–3209.
French, H. M. (2007), *The Periglacial Environment*, John Wiley, The Atrium, Southern Gate, Chichester, U. K.
Gessler, P. E., I. D. Moore, N. J. McKenzie, and P. J. Ryan (1995), International soil-landscape modeling and spatial prediction of soil attributes, *J. Geogr. Inf. Syst.*, *9*, 421–432.
Gessler, P. E., O. A. Chadwick, F. Chamran, L. Althouse, and K. Holmes (2000), Modeling soil-landscape and ecosystem properties using terrain attributes, *Soil Sci. Soc. Am.*, *64*, 2046–2056.
Gilmanov, T. G., and W. C. Oechel (1995), New estimates of organic matter reserves and net primary productivity of the North American tundra ecosystems, *J. Biogeogr.*, *2*, 723–741.
Gomez, C., R. A. Viscarra Rossel, and A. B. McBratney (2008), Soil organic carbon prediction by hyperspectral remote sensing and field vis-NIP spectroscopy: An Australian case study, *Geoderma*, *146*, 403–411.
Gorham, E. (1991), Northern Peatlands: Role in the carbon cycle and probable responses to climate warming, *Ecol. Appl.*, *1*, 182–195.
Graniero, A. P., and J. S. Price (1999), The importance of topographic factors on the distribution of bog and heath in a Newfoundland blanket bog complex, *Catena*, *36*, 233–254.
Grosse, G., et al. (2011), Vulnerability of high-latitude soil organic carbon in North America to disturbance, *J. Geophys. Res.*, *116*, G00K06, doi:10.1029/2010JG001507.
Hayes, D. J., D. W. Kicklighter, A. D. McGuire, M. Chen, Q. Zhuang, F. Yuan, J. M. Melillo, and S. D. Wullschleger (2014), The impacts of recent permafrost thaw on land-atmosphere greenhouse gas exchange, *Environ. Res. Lett.*, *9*, 045005, doi:10.1088/1748-9326/9/4/045005.
Hicken, E. J. (1974), The development of meanders in natural river channels, *Am. J. Sci.*, *274*, 414–442.
Higuera, P. E., M. L. Chipman, J. L. Barnes, M. A. Urban, and F. S. Hu (2011), Variability of tundra fire regimes in Arctic Alaska: Millennial scale patterns and ecological implications, *Ecol. Appl.*, *21*, 3211–3226.
Hu, F. S., P. E. Higuera, J. E. Walsh, W. L. Chapman, P. A. Duffy, L. B. Brubaker, and M. L. Chipman (2010), Tundra burning in Alaska: Linkages to climatic change and sea-ice retreat, *J. Geophys. Res.*, *115*, G04002, doi:10.1029/2009JG001270.
Intermap (2010), *Product Handbook and Quick Start Guide*, vol. 4.4, Standard ed., Quadrant: Howard Pass, C1, Northwest.
Jensen, A. E., K. A. Lohse, B. T. Crosby, and C. I. Mora (2014), Variations in soil carbon dioxide efflux across a thaw slump chronosequence in northwestern Alaska, *Environ. Res. Lett.*, *9*, 025001, doi:10.1088/1748-9326/9/2/025001.
Johnson, K. D., et al. (2011), Soil carbon distribution in Alaska in relation to soil forming factors, *Geoderma*, *167–168*, 71–84.
Johnson, K. D., J. Harden, A. D. McGuire, M. Clark, F. Yuan, and A. O. Finley (2013), Permafrost and organic layer interactions over a climate gradient in a discontinuous permafrost zone, *Environ. Res. Lett.*, *8*, 12.
Jones, B. M., A. L. Breen, B. V. Gaglioti, D. H. Mann, A. V. Rocha, G. Grosse, C. D. Arp, M. L. Kunz, and D. A. Walker (2013), Identification of unrecognized tundra fire events on the north slope of Alaska, *Biogeosciences*, *118*, 1334–1344.
Jorgenson, M. T., V. Romanovsky, J. Harden, Y. Shur, J. O'Donnell, E. A. Shuur, M. Kanevskiy, and S. Marchenko (2010), Resilience and vulnerability of permafrost to climate change, *Can. J. For.*, *40*, 1219–1236.
Kurz, W. A., M. J. Apps, T. M. Webb, and P. J. McNamee (1992), The carbon budget of the Canadian forest sector: Phase 1 For. Can., Northwest Reg., North. For. Cent., Edmonton, Alberta. Inf. Rep. NOR-X-326.
Lantuit, H., W. H. Polland, N. Couture, M. Fritz, L. Schirrmeister, H. Meyer, and H. W. Hubberten (2012), Modern and Late Holocene retrogressive thaw slump activity on the Yukon Coastal Plain and the Herschel Island, Yukon Territory, Canada, *Permafrost Periglacial Process.*, *23*, 39–51.
Mack, M. C., M. Syndonia Bret-Harte, T. N. Hollingsworth, R. R. Jandt, E. A. G. Schuur, G. R. Shaver, and D. L. Verbyla (2011), Carbon loss from an unprecedented Arctic tundra wildfire, *Nat. Res. Lett.*, *475*, 489–492.
Marchenko, S., V. Romanovsky, and G. Tipenko (2008), Numerical modeling of spatial permafrost dynamics in Alaska, in *Proceedings of the Ninth International Conference on Permafrost*, vol. 2, pp. 1125–1130, Univ. of Alaska, Fairbanks, Jun 29–July 3, 2008.
McGuire, A. D., et al. (2012), An assessment of the carbon balance of Arctic tundra: Comparisons among observations, process models, and atmospheric inversions, *Biogeosciences*, *9*, 3185–3204.
Michaelson, G. J., C. L. Ping, H. Epstein, J. M. Kimble, and D. A. Walker (2008), Soils and frost boil ecosystems across the North American Arctic Transect, *J. Geophys. Res.*, *113*, G03S11, doi:10.1029/2007JG000672.
Michaelson, G. J., C. L. Ping, and M. Clark (2013), Soil pedon C and N data for Alaska: An analysis and update, *Open J. Soil Sci.*, *3*, 132–142.
Mishra, U., and W. J. Riley (2012), Alaska soil carbon stocks: Spatial variability and dependence on environmental factors, *Biogeosciences*, *9*, 3637–3645.
Mishra, U., et al. (2013), Empirical estimates to reduce modeling uncertainties of soil organic carbon in permafrost regions: A review of recent progress and remaining challenges, *Environ. Res. Lett*, *8*, 035020, 9.
Molenaar, C. R., R. M. Egbert, and L. F. Krystinik (1988), Depositional facies, petrography, and reservoir potential of the Fortress Mountain formation (lower cretaceous) central North Slope, Alaska, Geology and Exploration of the National Petroleum Reserve in Alaska 1974–82, *U.S. Geol. Surv. Prof. Pap. 1399*.
Nanson, G. C. (1980), Point bar floodplain formation of the meandering Beatton River, northeastern British Columbia, Canada, *Sedimentology*, *27*, 3–29.
Niu, F., J. Luo, Z. Lin, W. Ma, and J. Lu (2012), Development and thermal regime of a thaw slump in the Qinghai-Tibet plateau, *Cold Reg. Sci. Technol.*, *83–84*, 131–138.
Nowacki, G., P. Spencer, M. Fleming, T. Brock, and T. Jorgenson (2001), Ecoregions of Alaska: 2001, *U.S. Geol. Surv. Open File Rep., 02–297*, (Region Descriptions).
Panikov, N. S., P. W. Flanagan, W. C. Oechel, M. A. Mastepanov, and T. R. Christensen (2006), Microbial activity in soils frozen to below −39°C, *Soil Biol. Biogeochem.*, *38*, 785–794.
Parry, L. E., D. J. Charman, and J. P. W. Noades (2012), A method for modeling peat depth in blanket peatlands, *Soil Use Manage.*, *28*, 614–624.
Pastick, N. J., M. Rigge, B. K. Wylie, M. T. Jorgenson, J. R. Rose, K. D. Johnson, and L. Ji (2014), Distribution and landscape controls of organic layer thickness and carbon within the Alaskan Yukon River Basin, *Geoderma*, *230–231*, 79–94.
Ping, C. L., J. G. Bockheim, J. M. Kimble, G. L. Michaelson, and D. A. Walker (1998), Characteristics of cryogenic soils along a latitudinal transect in Arctic Alaska, *J. Geophys. Res.*, *103*, 28,917–28,928, doi:10.1029/98JD02024.

Ping, C. L., G. J. Michaelson, M. T. Jorgenson, J. M. Kimble, H. Epstein, V. E. Romanovsky, and D. A. Walker (2008), High stocks of soil organic carbon in the North American Arctic Region, *Nat. Geosci.*, *1*, 615–619.

Price, P. B., and T. Sowers (2004), Temperature dependence of metabolic rates for microbial growth, maintenance, and survival, *Proc. Natl. Acad. Sci. U.S.A.*, *101*, 4631–4636.

Raynolds, M. K., D. A. Walker, K. J. Ambrosius, J. Brown, K. R. Everett, M. Kanevsky, G. P. Kofinas, V. E. Romanovsky, Y. L. Shur, and P. J. Webber (2014), Cumulative geoecological effects of 62 years of infrastructure and climate change in ice-rich permafrost landscapes, Prudhoe Bay Oilfield, Alaska, *Global Change Biol.*, *20*, 1211–1224.

Schaeffer, K., T. Zhang, L. Bruhwiler, and A. P. Barrett (2011), Amount and timing of permafrost carbon release in response to climate warming, *Tellus*, *63B*, 165–180.

Schuur, E. A. G., et al. (2008), Vulnerability of permafrost carbon to climate change: Implications for the global carbon cycle, *BioScience*, *58*, 701–714.

Schuur, E. A. G., et al. (2015), Climate change and the permafrost carbon feedback, *Nature*, *520*, 171–79.

Shaver, G. R., W. D. Billings, F. S. Chapin III, A. E. Giblin, K. J. Nadelhoffer, W. C. Oechel, and E. B. Rastetter (1992), Global change and the carbon balance of arctic ecosystems, *Biogeosciences*, *42*, 433–441.

Shur, Y. L., and M. T. Jorgenson (2007), Patterns of permafrost formation and degradation in relation to climate and ecosystems, *Permafrost Periglacial Process.*, *18*, 7–19.

Swanson, D. K., B. Lacelle, and C. Tarnocai (2000), Temperature and the boreal subarctic maximum in soil organic carbon, *Géogr. Phys. Quat.*, *54*, 157–167.

Tarnocai, C. (1998), The amount of organic carbon in various soil orders and ecological provinces in Canada, in *Soil Processes and the Carbon Cycle*, pp. 81–92, CRC Press LLC, Boca Raton, Fla.

Tarnocai, C., J. G. Canadell, E. A. G. Schuur, P. Kuhry, G. Mazhitova, and S. Zimov (2009), Soil carbon pools in the northern circumpolar permafrost region, *Global Biogeochem. Cycles*, *23*, GB2023, doi:10.1029/2008GB003327.

Treat, C. C., D. Wisser, S. Marchenko, and S. Frolking (2013), Modeling the effects of climate change and disturbance on permafrost stability in northern organic soils, *Mires Peat*, *12*, 1–17.

Tsai, C. C., Z. S. Chen, C. T. Duh, and F. W. Horng (2001), Prediction of soil depth using soil-landscape regression model: A case study on forest soils in Southern Taiwan, *Proc. Nat. Sci. Council, ROC(B)*, *25*, 34–39.

Walker, D. A. (2000), Hierarchical subdivision of Arctic tundra based on vegetation response to climate, parent material and topography, *Global Change Biol.*, *6*, 19–34.

Walker, D. A., et al. (2008), Arctic patterned-ground ecosystems: a synthesis of field studies and models along a North American Arctic Transect, *J. Geophys. Res.*, *113*, G03S01, doi:10.1029/2007JG000504.

Walker, M. D., D. A. Walker, K. R. Everett, and S. Charles (1989), Wetland soils and vegetation, Arctic Foothills, Alaska, *US Fish Wildlife Biol. Rep.*, *89*(7), 89.

Zuur, A. F., E. N. Leno, and C. S. Elphick (2010), A protocol for data exploration to avoid common statistical problems, *Methods Ecol. Evol.*, *1*, 3–14.